Entry System Options for Human Return from the Moon and Mars

Z. R. Putnam,[*] R. D. Braun,[†] and R. R. Rohrschneider[*]
Georgia Institute of Technology, Atlanta, Georgia, 30332

and

J. A. Dec[‡]
NASA Langley Research Center, Hampton, Virginia, 23681

Earth entry system options for human return missions from the Moon and Mars were analyzed and compared to identify trends among the configurations and trajectory options and to facilitate informed decision making at the exploration architecture level. Entry system options included ballistic, lifting capsule, biconic, and lifting body configurations with direct entry and aerocapture trajectories. For each configuration and trajectory option, the thermal environment, deceleration environment, crossrange and downrange performance, and entry corridor were assessed. In addition, the feasibility of a common vehicle for lunar and Mars return was investigated. The results show that a low lift-to-drag ratio (L/D = 0.3) vehicle provides sufficient performance for both lunar and Mars return missions while providing the following benefits: excellent packaging efficiency, low structural and TPS mass fraction, ease of launch vehicle integration, and system elegance and simplicity. Numerous configuration options exist that achieve this L/D.

Nomenclature

α	=	angle of attack
β	=	ballistic coefficient
γ	=	flight-path angle
L/D	=	lift-to-drag ratio
LEO	=	low Earth orbit
SRC	=	sample return capsule
CEV	=	Crew Exploration Vehicle
STS	=	Space Transportation System
TPS	=	thermal protection system

I. Introduction

THE renewed interest in human exploration beyond low earth orbit has led to many different viewpoints on what exploration architecture is appropriate for human missions to the Moon and Mars. While numerous exploration architectures exist, most require high-speed, aeroassisted deceleration of a crewed vehicle at Earth. There are many possible options for the entry system, and selection among these options will have a significant effect on the overall exploration architecture. The entry system is typically carried through an entire mission, and therefore its mass, size and complexity can have a large impact on other architectural elements. This study seeks to compare a broad range of entry system options for high speed entry at Earth to facilitate competent selection at the architecture level.

Entry system selection for future human exploration architectures will likely be based on different criteria than used in design of the only previous such system, the Apollo Command Module (CM). The design driver for the amount of lift generated by the Apollo CM was navigation error at atmospheric interface—the required lift-to-drag

---

[*] Graduate Research Assistant, School of Aerospace Engineering, 270 Ferst Drive, AIAA Student Member.
[†] Associate Professor, School of Aerospace Engineering, 270 Ferst Drive, AIAA Associate Fellow.
[‡] Thermal Engineer, Structural and Thermal Systems Branch, 1 N. Dryden Street, MS 431.

ratio required was 0.25[1]. Today, significant improvements in Earth approach navigation significantly reduce the requirements for lift. In addition, the Apollo CM guidance was designed to allow a maximum deceleration of 12g's during nominal entry[2]. Typical Apollo missions reached peak decelerations over 6.5g's during entry[3]. With a long-term focus on human exploration of Mars, Lunar mission durations will be significantly longer than the Apollo program to prepare for multi-year missions to Mars. These missions will subject astronauts to micro and low gravity for long periods of time and may require more stringent limits on deceleration during Earth entry than used in the Apollo program to ensure the safety of physiologically deconditioned astronauts.

Aerocapture guidance was a flight option for the Apollo program, which required a lift-to-drag ratio of 0.25, although it was never used[1]. Previous work on the aerocapture Mars return mission by Braun, Powell and Lyne advocates a minimum lift-to-drag requirement of 0.5 [4]. However, it was assumed that a large corridor (0.5°-0.7°) was necessary for Mars return. Future corridor width requirements will be less stringent, allowing for lower lift-to-drag ratio vehicles to be used. In addition, the use of a single vehicle for both lunar and Mars return is an attractive option and this study seeks to investigate its feasibility by examining the increase in required lift-to-drag ratio necessary over lunar return requirements to support Mars return missions.

II. Approach

This study analyzed two types of aeroassist trajectories: direct entry and aerocapture. Direct entry uses a planetary atmosphere to decelerate the vehicle and land on the planet's surface (Figure 1a). Direct entry may occur from inbound hyperbolic trajectories or from orbit. Aerocapture uses a planetary atmosphere to decelerate a vehicle on an inbound hyperbolic trajectory. However, during aerocapture, the vehicle exits the atmosphere with the correct orbital energy to enter orbit around the planet (Figure 1b).
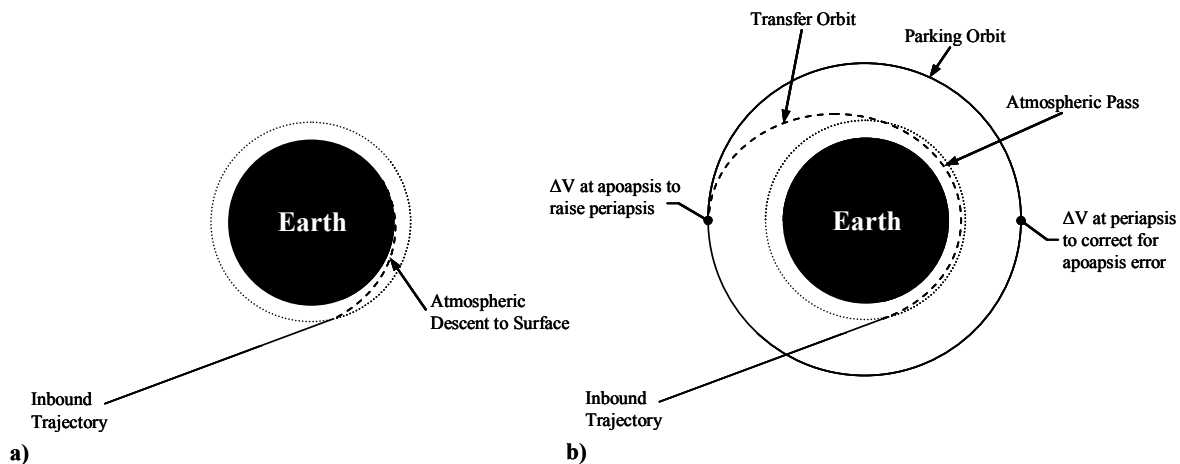

Figure 1. Aeroassist trajectories: (a) direct entry and (b) aerocapture.

A nominal Direct entry begins at atmospheric interface at 122 km (400000 ft) altitude with a given inertial velocity and flight path angle (Figure 2a). Atmospheric effects, including lift and drag, are negligible at this altitude. As the vehicle descends through the atmosphere, dynamic pressure increases quickly, causing hypersonic aerodynamics to dominate the vehicle dynamics. Aerodynamic forces decelerate the vehicle, and the vehicle quickly passes through peak heating and peak deceleration (Figure 2b, c). The magnitudes of the g-loading and heat rate can be mitigated through judicious use of lift generated by the vehicle. The constant altitude flight segment in Figure 2a is an example of this. When the vehicle decelerates to Mach 2, drogue chutes are released to ensure stability in the supersonic regime. Main chutes are deployed at approximately 1 km altitude after the vehicle bas become subsonic (Figure 2b). The main chutes reduce the vehicle's velocity to approximately 8 m/s. This is consistent with the Apollo program, whose splashdown velocity was approximately 31 ft/s (9.44 m/s). [5] This study does not model the terminal descent or touchdown phase of direct entry.

A nominal aerocapture trajectory also begins at atmospheric interface at 122 km altitude. The vehicle enters the atmosphere and begins to decelerate as aerodynamic forces act on the vehicle (Figure 3a). The vehicle then uses lift control to dissipate the correct amount of energy and exit the atmosphere in a given orbit. At peak deceleration, the vehicle uses lift control to fly a constant altitude segment in the atmosphere (Figure 3b). At the proper time, the vehicle switches to a full lift-up orientation to exit the atmosphere with the proper orbital energy (Figure 3a).

American Institute of Aeronautics and Astronautics

A variety of techniques can be used to mitigate the high heating rates and g-loads experienced during direct entry and, to a lesser extent, during aerocapture. This study focused exclusively on lift control through bank angle modulation. Changes in bank angle are achieved propulsively through a reaction control system.
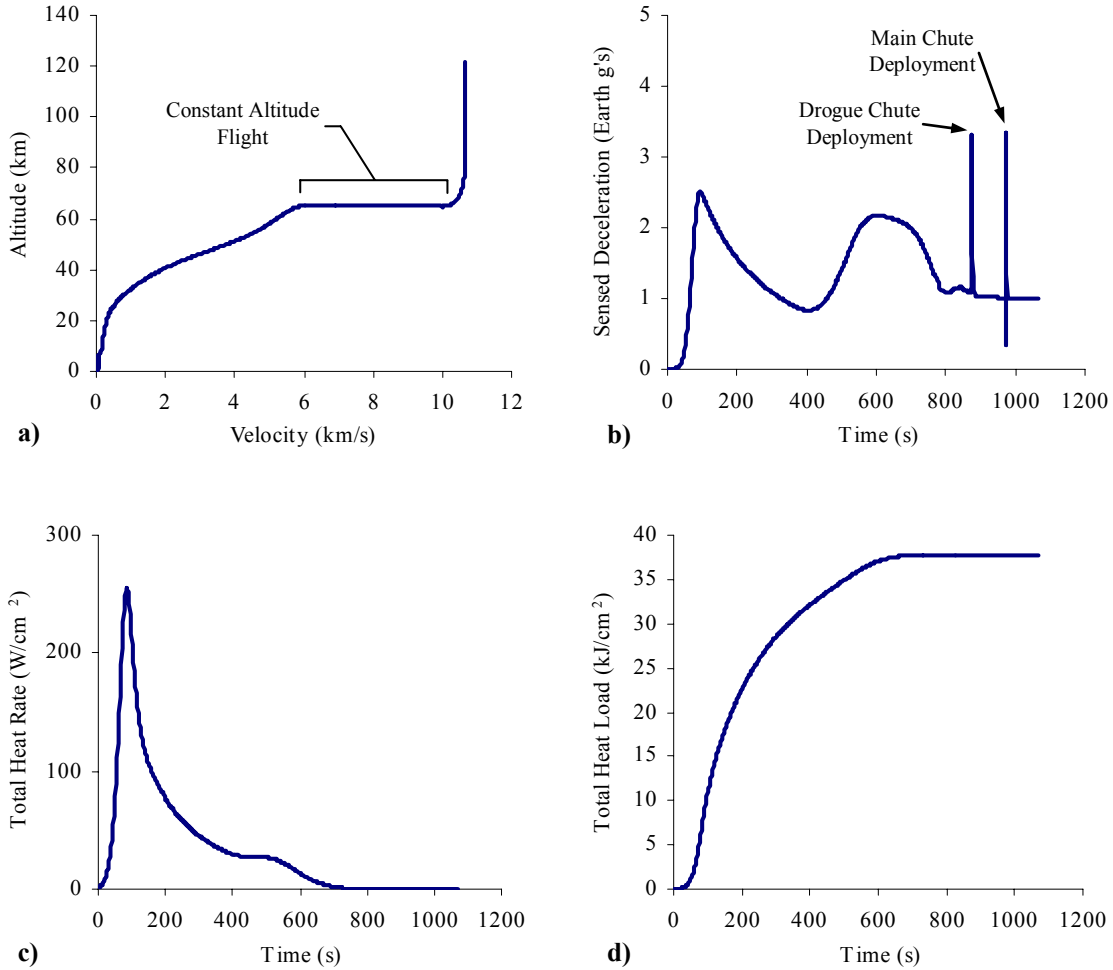

Figure 2. Nominal direct entry trajectory, L/D = 0.3, β = 365 kg/m², γ = -5.61°: (a) altitude versus velocity, (b) sensed deceleration versus time, (c) heat rate versus time and (d) integrated heat load versus time.
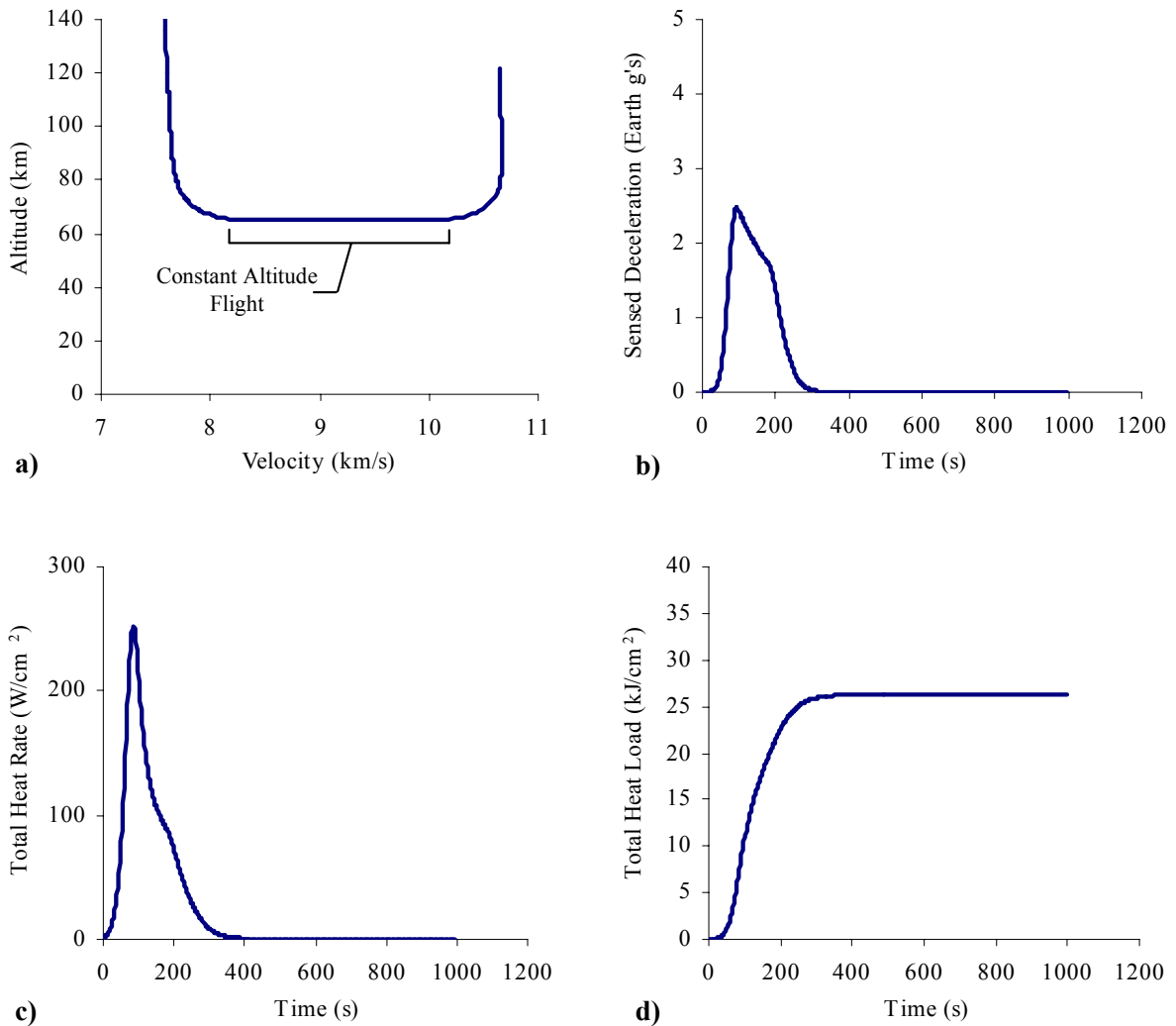
Figure 3. Nominal aerocapture trajectory, L/D = 0.3, β = 365 kg/m², γ = -5.60°: (a) altitude versus velocity, (b) sensed deceleration versus time, (c) heat rate versus time and (d) integrated heat load versus time.

A. Entry Corridor Definition

For a given inertial velocity at atmospheric interface, there are many possible trajectories that satisfy a given set of constraints. For direct entry, the trajectory is constrained to remain in the atmosphere until the vehicle reaches the surface. For aerocapture, the trajectory is constrained to meet a given energy at atmospheric exit. Variation within these constraints may be achieved by re-orienting the lift vector of the vehicle through bank angle modulation. For direct entry, if the initial flight path angle is too shallow, the vehicle will skip out of the atmosphere. The shallowest possible flight path angle for which the vehicle can reach the surface defines the upper boundary of the aerodynamic corridor. The steepest possible flight path angle for which the vehicle will achieve direct entry is 90°. This represents the lower boundary of the aerodynamic corridor. For aerocapture, if the initial flight path angle is too shallow, not enough energy will be dissipated during the atmospheric pass. If the flight path angle is too steep, too much energy will be dissipated. The shallowest and steepest possible flight path angles for which the correct amount of energy is dissipated are the upper and lower aerodynamic corridor boundaries, respectively. The locus of all possible trajectories defined by the upper and lower boundaries for direct entry and aerocapture is known as the aerodynamic entry corridor.

In addition to the previously mentioned constraints, additional requirements may be imposed on entry trajectories that define a flyable or operational corridor. Such constraints may include limits on the peak heat rate,

American Institute of Aeronautics and Astronautics

total integrated heat load, or on the peak deceleration. Peak heat rate and peak deceleration typically limit the lower, or steep corridor boundary, while limits on the integrated heat load will limit the upper or shallow boundary. For this study, a peak deceleration limit of 5 Earth g's was imposed.

Sample corridors are shown in Figure 5 and Figure 4 for direct entry and aerocapture. For direct entry, the upper corridor boundary is achieved with a lift-down orientation, followed by constant altitude flight to reduce peak deceleration. The lower aerodynamic corridor boundary is achieved with a lift-up orientation and a 90° flight path angle. The lower flyable corridor boundary is achieved with a lift-up orientation and constant deceleration flight to limit peak deceleration. For aerocapture, the upper corridor boundary is achieved with a lift-down orientation throughout the trajectory. The lower boundary of the corridor is achieved with a lift-up orientation. The flyable corridor is further limited by a peak deceleration limit. The boundary of the flyable corridor is achieved with a lift-up orientation followed by bank angle modulation to achieve the required exit energy.
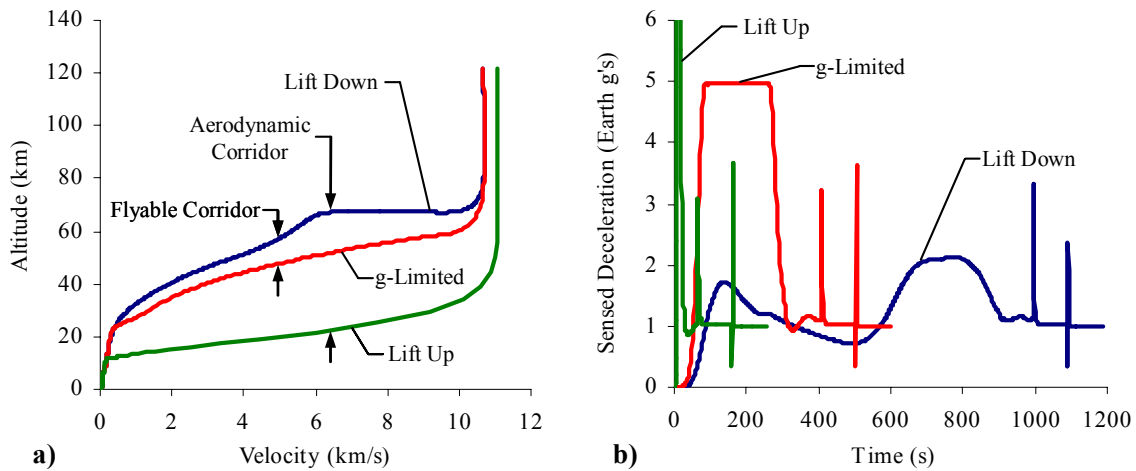

Figure 5. Sample direct entry corridor trajectories, L/D = 0.3, β = 365 kg/m^2: (a) altitude versus relative velocity and (b) sensed deceleration versus time.

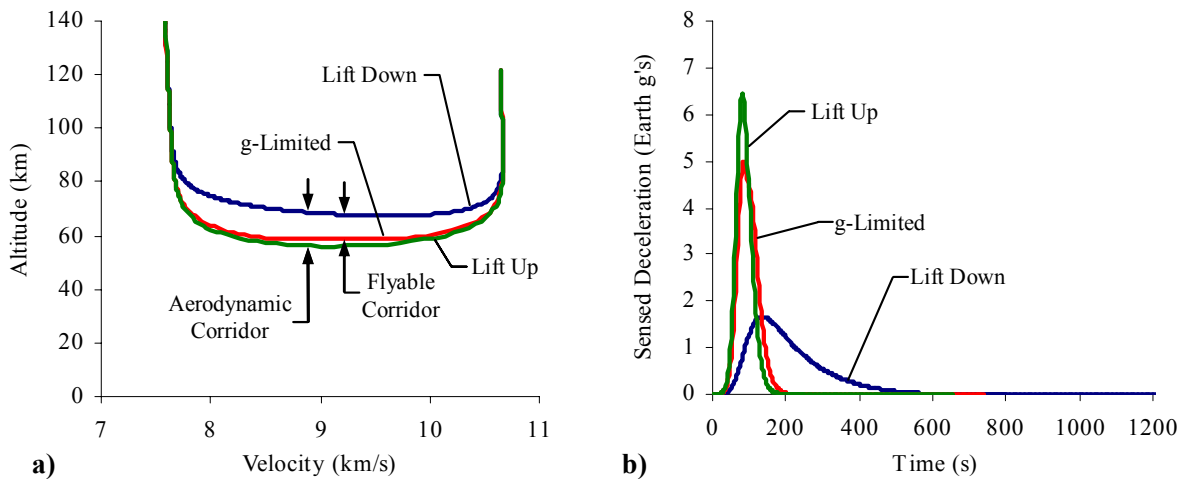**Figure 4. Sample aerocapture corridor trajectories, L/D = 0.3, β = 365 kg/m^2: (a) altitude versus relative velocity and (b) sensed deceleration versus time.**

B. Trajectory Requirements

To facilitate a comparative analysis, deceleration and corridor width requirements were imposed on all trajectories simulated in this study. It should be noted that no requirements were imposed on vehicle angular rates.

1. Peak Deceleration Limit

While NASA has not specified deceleration requirements for a crewed entry vehicle, it is desirable to limit the peak deceleration for the human crew. Reducing the peak deceleration becomes more important for crews that have been in a low gravity or microgravity environment for an extended period of time, such as on return from extended duration lunar missions or Mars missions. This study adopted a maximum peak deceleration limit of five Earth g's, or 45.05 m/s^2. This value is consistent with current literature on human missions to the Moon and Mars as well as with Soviet experience with the Soyuz entry vehicle returning crews from extended duration missions on Mir[6]. No limit was placed on the duration of peak deceleration.

2. Entry Corridor Width

The flyable entry corridor was defined to be the difference in inertial flight path angle between the shallowest possible entry, at the skip-out boundary, and the steepest possible entry, limited by peak deceleration requirements. For the purposes of this study, the minimum entry corridor width was assumed to be 0.4°. This conservative estimate is derived from recent entry uncertainty analyses used in the Stardust and Genesis sample return missions[7,8]. The uncertainty requirement in the inertial flight path angle at atmospheric interface for the Stardust and Genesis sample return capsules (SRCs) was 0.16°. For a crewed mission, additional conservatism is warranted. A corridor width of 0.4°, more than double the Stardust and Genesis SRC values, provides significant conservatism, greatly reducing the level of risk in any human exploration architecture entry system.

3. Skipping Trajectories

In addition, skipping trajectories were not considered for direct entry. The vehicle was constrained to remain below atmospheric interface (122 km altitude) after entry.

4. Aerocapture Parking Orbits

For this study, all aerocapture trajectories captured into a transfer orbit with an orbital energy of -30 km^2/m^2. This transfer orbit allows direct insertion into LEO. While capturing into higher orbits is possible and reduces the amount of energy that must be dissipated during the atmospheric pass, capturing into LEO offers several benefits for crewed vehicles: LEO orbits do not involve multiple passes through eh Van Allen radiation belts and they facilitate rendezvous with the ISS and other orbiting infrastructure.

C. Vehicle Concepts

A set of vehicle concepts representing a broad range of options was selected for this study. The set includes moldlines with lift-to-drag ratios ranging from 0 to approximately 1.4. The optimum vehicle moldlines for lunar and Mars return missions depends on many factors, including range, deceleration, and aeroheating performance; packaging; complexity; and cost. Each vehicle in the set represents a different balance of these factors. The set of vehicles includes a ballistic capsule, a low lift capsule, the Apollo CM[9], an axis-symmetric biconic, and a simple lifting body[16], shown in

. The aerodynamics data for the Apollo CM were obtained from Ref. 9. The lifting body and biconic aerodynamics data were obtained through computational methods.

The biconic and lifting body vehicles offer the highest lift-to-drag ratios but are more massive and complex. The capsule vehicles offer low complexity and low mass at the expense of lift-to-drag ratio.
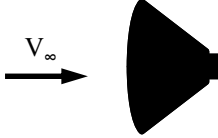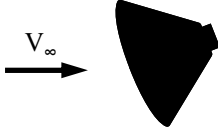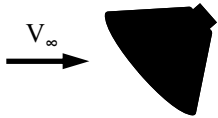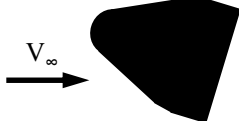
Vehicle Name	Vehicle Moldline	Description
Ballistic Capsule	V_∞	Lift-to-drag ratio: 0.0 at $\alpha = 0°$ Nose radius: 3 m Mass: 5500 kg Apollo Command Module aerodynamics.
Low-lift Capsule	V_∞	Lift-to-drag ratio: 0.1 at $\alpha = -10°$ Nose radius: 3 m Mass: 5500 kg Apollo Command Module aerodynamics.
Apollo Capsule	V_∞	Lift-to-drag ratio: 0.3 at $\alpha = -25°$ Nose radius: 3 m Mass: 5500 kg Apollo Command Module aerodynamics.
Biconic	V_∞	Lift-to-drag ratio: 0.55 at $\alpha = 25°$ Nose radius: 2 m Mass: 8000 kg Biconic CEV concept from Draper Labs/M.I.T. CE+R study. Aerodynamic data generated in APAS.
Lifting Body	V_∞	Lift-to-drag ratio: 1.4 at $\alpha = 25°$ Nose Radius: 2 m Mass: 8000 kg Simple lifting body CEV concept. Aerodynamic data generated in APAS.

Figure 6. Vehicle types analyzed.

An Apollo-style parachute system was used during the terminal descent phase for each of the vehicles. This system consists of two mortar-deployed drogues and three mortar-deployed main parachutes. Nominal velocity at touchdown is approximately 8 m/s. Relevant information for the parachute system is given in Table 1.

Table 1.   Relevant parachute parameters.[10]

Parameter	Drogues	Main Parachutes
Number of Parachutes	2	3
Type	Supersonic Drogue	Ringsail
Drag Coefficient	0.55	0.85
Inflated Diameter	5.0 m	25.4 m

D. Computational Methods

Aerodynamic analysis for the biconic and lifting body vehicles was performed using the Aerodynamic Preliminary Analysis System (APAS)[11]. The fidelity of the APAS hypersonic aerodynamic analyses was of a similar order as other computational methods used in this study.

The analysis of atmospheric entry at Earth was performed with the three-degree-of-freedom version of the Program to Optimize Simulated Trajectories (POST)[12]. Several important features of POST were utilized, including the parachute drag model and the linear feedback control option. The linear feedback control option was used to fly constant altitude and constant deceleration entry trajectories.

Aeroheating calculations were performed with two stagnation point heating approximation methods. Convective heating was calculated using Chapman's equation[13]. Radiative heating was calculated using the Tauber-Sutton

approximation for Earth entry[14]. The results for both calculations were summed to find the total stagnation point heat rate and heat load as a function of time for each trajectory.

Forebody heat shield sizing was performed with the Charring Material Thermal Response and Ablation Program (CMA)[15]. CMA is a finite difference computational tool used to compute the 1-D transient thermal response of a 3-D isotropic material that can ablate from the surface and decompose in-depth.

E. Parameter Ranges

Planetary entry trades can be largely parameterized across the following four key design variables: atmospheric entry velocity magnitude, atmospheric entry velocity flight-path angle, vehicle ballistic coefficient and vehicle lift-to-drag ratio.

Inertial velocity at atmospheric interface was varied throughout the study from 7 to 14 km/s. A 7 km/s entry corresponds to entry from LEO, 11 km/s to lunar return, 12.5 to 14 km/s to Mars return. 12.5 to 14 km/s represent a range of expected entry velocities across mission opportunities and Mars return transit times, with 14 km/s allowing return durations of 200 days or less in all opportunities, as shown in Figure 7. All trajectories used the Apollo 11 state vector (see Table 2) at atmospheric interface, with variations in flight path angle and inertial velocity only.

While multiple definitions exist for ballistic coefficient (β), in this study β was defined as the mass of the vehicle divided by the product of its hypersonic drag coefficient and aerodynamic reference area. Ballistic coefficient was varied by scaling the mass of a given vehicle. In select analyses, β was varied between 200 and 600 kg/m^2.

Table 2. Apollo 11 state vector at atmospheric interface.

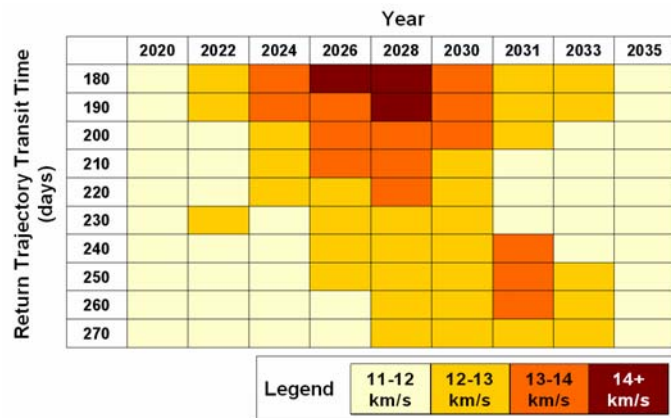| Parameter	Value
Azimuth	50.18°
Longitude	171.96° W
Latitude	-3.19° N
Altitude	121920 m

Figure 7. Mars return velocity as a function of year and transit time.

III. Results and Discussion

A. Direct Entry Deceleration Performance

Figure 8 shows the hypersonic lift-to-drag ratio required to satisfy a prescribed peak deceleration limit and a 0.4° entry corridor width for direct entry. The figure shows that a significant decrease in peak deceleration can be obtained with a small amount of lift. For example, at lunar return speeds (11 km/s), a lift-to-drag ratio of 0.65 reduces the peak deceleration to about 2g (Figure 9). This is a significant improvement over the ballistic capsule peak deceleration of 8g. Note that a lift-to-drag ratio of 0.3 can achieve a 5g deceleration limit even at very high velocity (14 km/s). With lift-to-drag ratio of 0.4, a 3.5g limit can be achieved for all but the highest velocities, whereas the lift-to-drag ratio must be increased to 1 or more to reduce the peak deceleration to 2g. This shows that the deceleration performance difference between a capsule (L/D ≈ 0.3-0.4) and a lifting body (L/D ≥ 1) is very small. Note that if navigation accuracy were improved beyond the 0.4° entry corridor conservatively
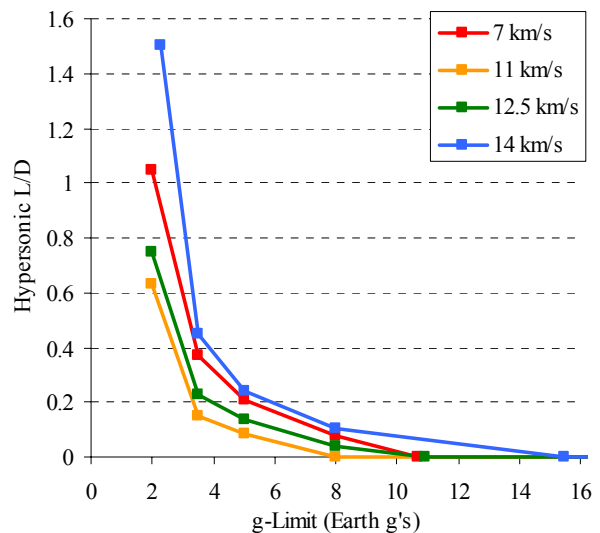

Figure 8. Required lift-to-drag ratio for a given g-limit for direct entry.

assumed, an even lower lift-to-drag ratio vehicle would be required.

Figure 8 also shows that more lift-to-drag ratio is required to maintain a given deceleration limit for low velocity entry at 7 km/s than for lunar return velocity. This is caused by the loss of aerodynamic control authority due to the reduced dynamic pressure associated with a lower entry velocity.
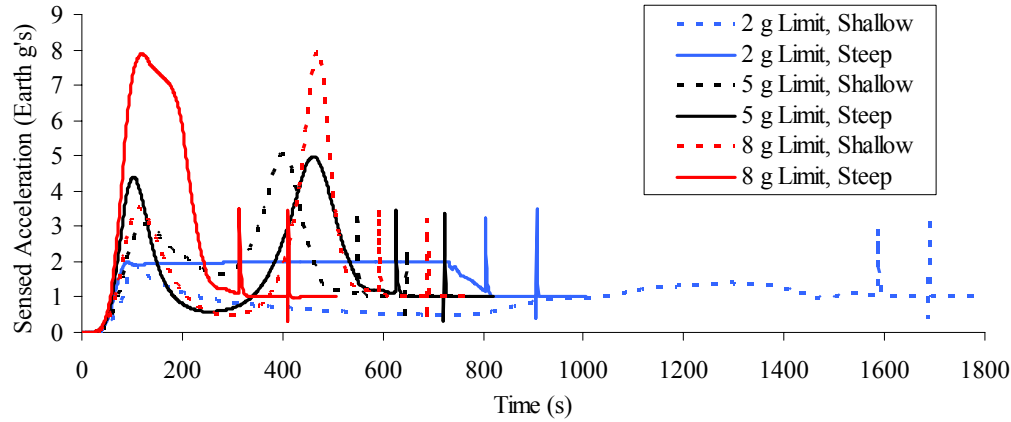

Figure 9. Deceleration profiles for several g-limits for direct entry at 11 km/s.

B. Direct Entry Corridor

The entry corridor width was determined for several entry velocities, ballistic coefficients, and vehicle types for direct entry, as shown in Figure 10. The data show that the most influential parameter in determining corridor width is the vehicle lift-to-drag ratio. The lifting body corridor width is approximately twice that of the lifting capsule, due to its much higher lift-to-drag ratio. In contrast, ballistic coefficient does not have a large effect on corridor width, especially at high entry velocities. As expected, corridor width decreases significantly with increasing entry velocity because of the 5g deceleration limit. However, it should be noted that both the lifting capsule and the lifting body possesses adequate corridor performance at entry velocities as high as 14 km/s. While a larger corridor is desirable, it is only desirable from the standpoint that a larger corridor allows greater uncertainty in interplanetary navigation and entry system flight control. However, current robotic missions returning to Earth in this entry velocity

Figure 10.   Direct entry corridor width for several vehicles.

range have demonstrated high accuracy interplanetary navigation techniques that reduce the required corridor width below that assumed in this study. For example, for a corridor width of 0.16°, such as that demonstrated by the Stardust and Genesis SRCs, lift-to-drag ratio values less than 0.1 will provide acceptable performance, as shown in Figure 10.
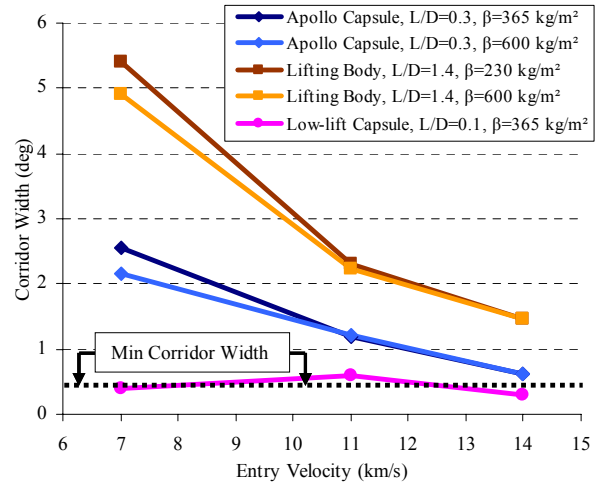
In conclusion, for a corridor width of 0.4 deg, a lift-to-drag ratio of 0.1 provides sufficient control authority for lunar return speeds. A lift-to-drag ratio of 0.3 provides sufficient control authority with margin for Earth return velocities below 14 km/s.

C. Direct Entry Range Performance

The range performance of a lifting capsule and a lifting body were compared over several ballistic coefficients for direct entry trajectories. The primary figures of merit for range performance are the maximum downrange and maximum crossrange capability of a vehicle at a given entry velocity. Downrange is defined as the distance traveled

during entry within the orbital plane. Crossrange is defined as the distance traveled perpendicular to the orbital plane. Table 3 shows the range performance for several vehicles at lunar return velocity. Clearly, the range capability of the lifting body was superior. However, the lifting capsule still possesses significant capability, especially if skipping trajectories are employed. This was an option that was flight-certified, but never used, in the Apollo program [REF]. Ballistic coefficient has only a small effect on range performance.

Table 3.   Direct Entry Range Capabilities at Lunar Return Velocities.

Vehicle	Ballistic Coefficient (kg/m^2)	Downrange Capability (km)		Crossrange Capability (km)	
		Minimum	Maximum	Minimum	Maximum
Lifting Capsule L/D = 0.3	200	1811	5199	0	210
	365	1845	5174	0	209
	600	1870	4573	0	200
…with skipping	365	2000	8500+	0	1000+ km
Lifting Body L/D = 1.4	200	2053	19747	0	4509
	400	2095	19910	0	4370
	600	2123	20780	0	4152

Adequate mission design and orbital operations flexibility, in the form of appropriate selection of departure dates and times and judicial use of in-space propulsive capability provide for minimal downrange and crossrange requirements for lunar and Mars return. In the absence of military operational requirements, such as those dictated for STS, only a modest amount of reach capability necessary for uncertainty mitigation is required for a crewed entry vehicle. This capability is achievable with both capsules and lifting bodies.

D. Direct Entry Aeroheating
The aeroheating environment dictates the type and size of the thermal protection system (TPS) that must be used for an entry vehicle. Peak heat rate generally determines the range of possible TPS materials while the integrated heat load determines the thickness and mass of the TPS. Heat rate and integrated heat load calculations were performed with engineering analysis techniques that address both convective and radiative heating contributions.

Figure 11 shows the maximum heat loads and maximum peak heat rates for 5g-limited direct entry trajectories. The maximum peak heat load is incurred at the shallow corridor boundary, while the maximum peak heat rate is incurred at the steep corridor boundary. The results include both convective and radiative heating. For blunt bodies entering at lunar return velocities (11 km/s) and greater, peak stagnation-point heat rates are high, approximately 300 W/cm^2 for lunar return and 1500 W/cm^2 for Mars return velocities. However, for lifting bodies, the peak heat
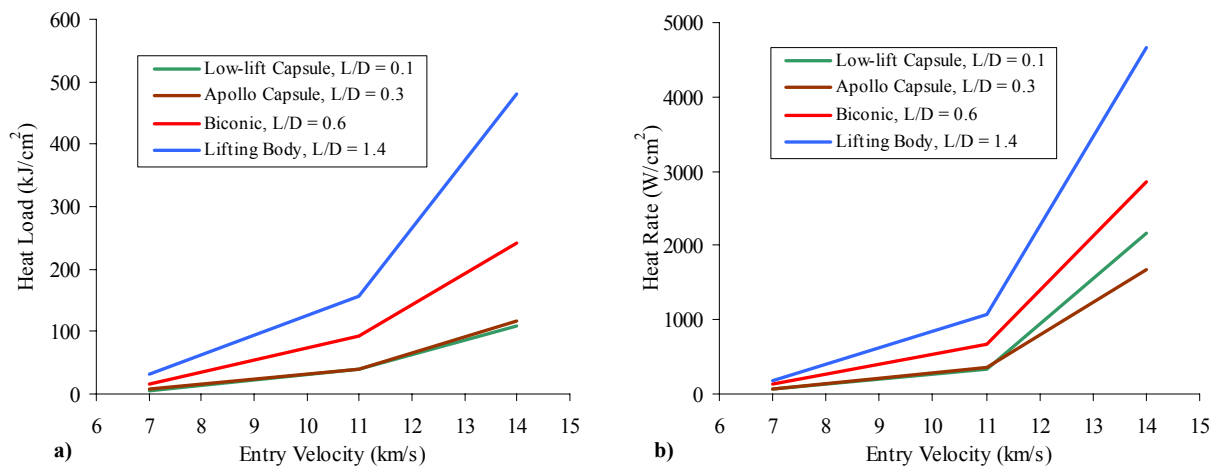

Figure 11.   Direct entry (a) maximum heat load and (b) maximum peak heat rate for several vehicles.

rates are even higher, with rates in excess of 4500 W/cm^2 for some Mars return velocities. These high heat rates are driven by the smaller nose radius of the lifting body and its ability to dive more steeply into the atmosphere while maintaining a 5g limit.

For the vehicles entering the Earth's atmosphere at speeds above 7 km/s, high heat rates demand an ablative or single-use heatshield. High heat loads can translate to a more massive TPS, as TPS thickness and mass may increase with increasing heat loads. This is in stark contrast to reusable TPS, such as that used by STS, where the integrated heat load does not have as strong an effect on TPS mass. Figure 12 shows the forebody heat shield mass as a function of entry velocity for two materials and several vehicles. The two materials are carbon phenolic, a material that can withstand heat rates in excess of 17 kW/cm^2 but is very heavy, and PICA, a material with a lower heat rate limit but a much lighter weight. These two materials represent bounding cases for the mass of the forward heat shield. In each case, the TPS mass is derived by assuming a constant thickness forebody heatshield sized to the stagnation-point heating environment, a conservative assumption. The lifting body and biconic vehicles require more massive heat shields due to their high heat loads and large surface areas. Note that total vehicle TPS mass includes the backshell heatshield and insulation which will also be larger for lifting and biconic vehicles than for capsules due to a more intense aeroheating environment and larger backshell TPS acreage.
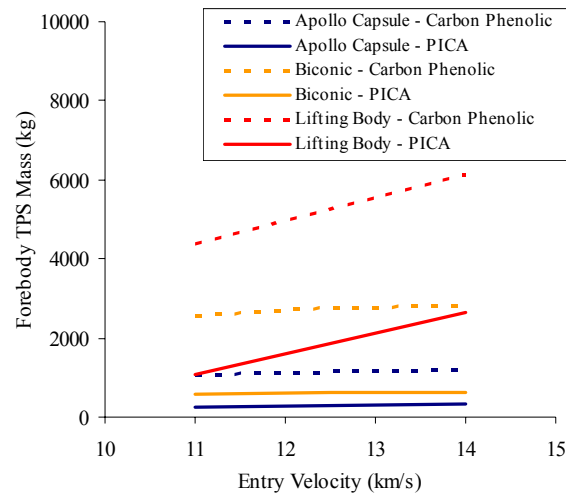

Figure 12.   Direct entry forebody heat shield masses for several vehicles.

Clearly, a blunt body offers a distinct TPS advantage over a lifting body. Both vehicle types require a non-reusable system for lunar return. A lifting body requires a higher performance TPS whose thickness and acreage requirements will lead to a more massive system. In contrast, a blunt body can utilize a lower performance material with a much lower total mass.

E. Aerocapture Deceleration Performance

Aerocapture trajectories typically exhibit low peak decelerations during the atmospheric pass when compared with direct entry trajectories. This is shown in Figure 13. For example, to limit deceleration to 5 g's at an entry velocity as high as 14 km/s, aerocapture requires a hypersonic lift-to-drag ratio of approximately 0.2. For direct entry, a hypersonic lift-to-drag ratio of about 0.3 is required for the same performance. A lift-to-drag ratio of 0.3 is capable of limiting deceleration to 4 g's up to 14 km/s. From Figure 13, it is readily apparent that increasing the aerocapture vehicle's lift-to-drag ratio beyond 0.3 provides a diminished performance return in performance. The reduction in peak deceleration at 14 km/s is only about 1 g when the lift-to-drag ratio is increased from 0.3 to 0.55. This reduction decreases with decreasing velocity—the benefit at 11 km/s is only 0.4 g.
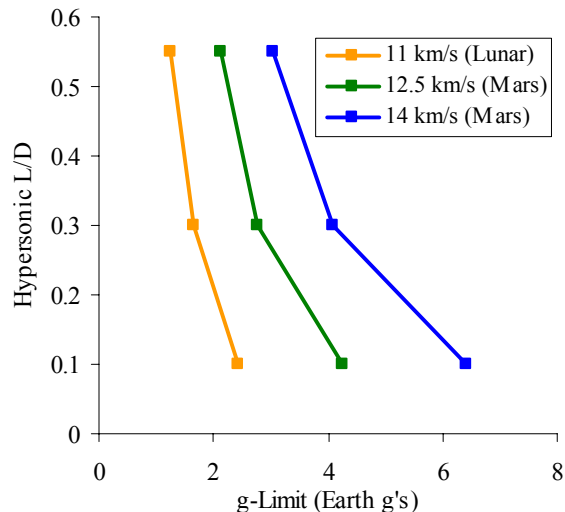

Figure 13.   Aerocapture g-limit versus required lift-to-drag ratio.

F. Aerocapture Corridor

The entry corridor was determined for three different vehicles for aerocapture. Ballistic coefficient was not varied, as it had only a small effect on the direct entry corridor widths. As for direct entry, aerocapture corridor width decreases as entry velocity increases, due to the imposed 5g peak deceleration constraint. The low-lift capsule (L/D = 0.1) provides acceptable performance for velocities lower than about 12 km/s. The Apollo capsule

(L/D = 0.3) and biconic vehicle (L/D = 0.55) provide adequate performance and substantial margin at velocities up to 14 km/s.

The sharp drop in biconic corridor width at high velocity is due to the relatively small drag coefficient of this vehicle. At high velocities, the biconic no longer generates enough drag to slow itself at sufficiently high altitude for the shallow corridor boundary. To increase the drag force on the vehicle and the associated energy dissipation, this vehicle must dive deeper into the atmosphere where the atmospheric density is much higher; however, the 5g deceleration constraint limits the flyable corridor. This is a primary disadvantage of biconic shapes over blunt bodies for high-speed deceleration—the high lift-to-drag ratios generated by the biconic shape are achieved by reducing the drag coefficient, not increasing the lift coefficient. While this provides additional control authority during hypersonic flight, it also requires that the

Figure 14. **Aerocapture corridor width for several vehicles.**

vehicle decelerate lower in the atmosphere where the density and resulting peak heat rate and peak deceleration are higher.

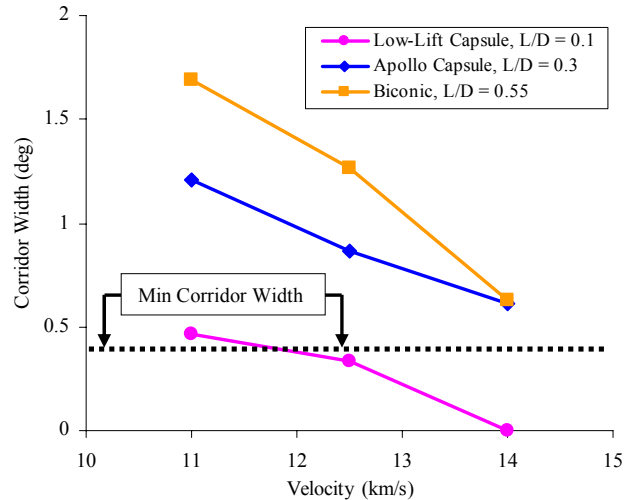## G. Aerocapture Range Performance
Range performance is generally not relevant to the aerocapture mission and was not analyzed.

H. Aerocapture Aeroheating
The aeroheating performance of several vehicles was calculated for nominal aerocapture trajectories. Figure 15 shows the maximum heat loads and maximum peak heat rates for 5g-limited aerocapture trajectories, with the maximum peak heat load incurred at the shallow corridor boundary and the maximum peak heat rate incurred at the steep corridor boundary. The results include both convective and radiative heating. The maximum heat rates for the aerocapture trajectories were only slightly less than those associated with direct entry. The total integrated heat loads were similar between both trajectory types. Similar to the direct entry data, the aerocapture heating data show that blunt bodies provide superior aeroheating performance. This is due to their large nose radii and high drag coefficients. Also, as expected, the total heat load and peak heat rate increase quickly with velocity at atmospheric interface. Ablative TPS is required for all velocities analyzed.
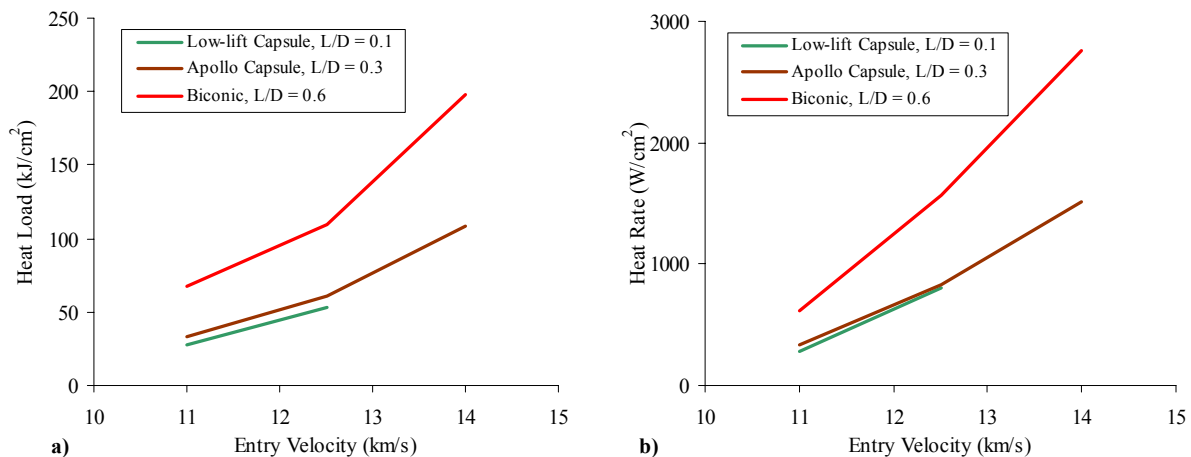

Figure 15. **Aerocapture (a) maximum heat load and (b) maximum peak heat rate for several vehicles.**

Forebody heat shields were sized for several vehicles for nominal aerocapture trajectories, shown in Figure 16. The masses of the aerocapture heat shields are similar to those for direct entry. Again, blunt bodies possess a distinct advantage over higher lift-to-drag ratio vehicles, such as the biconic. Forebody TPS masses for the biconic are three times that of the Apollo capsule and low-lift capsule for both PICA and carbon phenolic. This is largely due to the biconic's high integrated heat load and large TPS surface area. It should be noted that the TPS mass in Figure 16 does not include backshell TPS, the addition of which would probably increase the disparity between the Apollo capsule and the biconic.

Figure 16.   Aerocapture forebody heat shield masses for several vehicles.

IV. Conclusion

The performance capabilities of several Earth entry systems and trajectory options for human return from the Moon and Mars have been analyzed and compared. All vehicles considered, with exception of the ballistic vehicles, provide sufficient corridor width and deceleration performance for the lunar return mission for direct entry or aerocapture. Vehicles with lift-to-drag ratios greater than 0.2 provide acceptable performance for the Mars return mission for direct entry or aerocapture. It has been shown that high lift-to-drag ratio vehicles, such as a lifting body (L/D = 1.4), offer limited landing site access advantages over moderate lift-to-drag ratio capsules (L/D = 0.3). In contrast, moderate lift-to-drag capsules offer significant aeroheating and TPS advantages. The primary consideration for a lifting body vehicle is crossrange performance. Without a significant crossrange requirement (as provided by the U.S. Air Force in development of STS), a capsule vehicle configuration that generates a lift-to-drag ratio of 0.3 is not only sufficient, but provides significant mass, complexity and risk advantages.

In conclusion, a lifting capsule Earth entry system with L/D = 0.3 offers sufficient performance for Earth return from the Moon and Mars, while providing the following benefits: excellent packaging efficiency, low structural and TPS mass fraction, ease of launch vehicle integration and system elegance and simplicity. Numerous configuration options exist that achieve this L/D.

Acknowledgments

References

[1]Harpold, Jon C., "Minimum Lift-to-Drag Ratio Requirement for the Lunar Mission," NASA-TM-X-69752, October, 1967.

[2]Tolin, J. W., Harpold, J. C., and Rogers, J. E., "AS-503A/AS-504A Requirements for the RTCC: Reentry Phase," NASA-TM-X-69753, 1967.

[3]U.S. Manned Spacecraft Center Mission Evaluation Team, *Apollo 11 Mission Report*, NASA Scientific and Technical Information Office, Washington, D.C., 1971.

[4]Braun, R. D., Powell, R. W., and Lyne, J. E., "Earth Aerobraking Strategies for Manned Return from Mars," *Journal of Spacecraft and Rockets*, Vol. 29, No. 3, 1992, pp. 297-304.

[5]"Apollo 11 Lunar Landing Mission Press Kit", NASA, Washington, D.C., 1969, pp. 57-64, 90.

[6]Atkov, O. Y., personal communication, Head, All Union Cardiology Research Center, Moscow, Nov. 29, 1990.
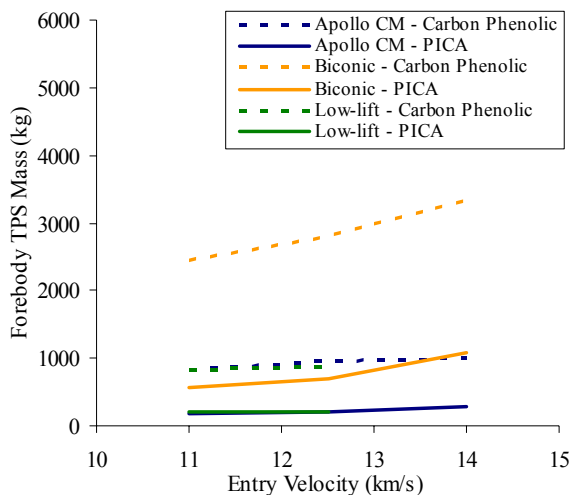
[7]Desai, Prasun N., Mitcheltree, Robert A., and Cheatwood, F. McNeil, "Entry Dispersion Analysis for the Stardust Comet Sample Return Capsule," *Journal of Spacecraft and Rockets*, Vol. 36, No. 3, 1999, pp.463-469.

[8]Desai, Prasun N. and Cheatwood, F. McNeil, "Entry Dispersion Analysis for the Genesis Sample Return Capsule," AAS/AIAA Astrodynamics Specialist Conference, August 1999, AAS 99-469.

[9]Graves, C. A. and Harpole, J. C., "Apollo Experience Report – Mission Planning for Apollo Entry," NASA TN D-6727, 1972.

[10]Knacke, T. W., Parachute Recovery Systems Design Manual, Para Publishing, Santa Barbara, CA, 1992, p. 5-4.

[11]Sova, G. and Divan, P., "Aerodynamics Preliminary Analysis System II, Part II – User's Manual," NASA CR 182077, April 1991.

[12]Brauer, G. L., Cornick, D. E., and Stevenson, R., "Capabilities and Applications of the Program to Optimize Simulated Trajectories (POST)," NASA CR-2770, Feb. 1977.

[13]Chapman, D. R., "An Approximate Analytical Method for Studying Entry into Planetary Atmospheres," NACA TN-4276, 1958.

[14]Tauber, M. E. and Sutton, K., "Stagnation-Point Radiative Heating Relations for Earth and Mars Entries," *Journal of Spacecraft and Rockets*, Vol. 28, No. 2, 1991, pp. 40-42.

[15]Anon., "User's Manual, Aerotherm Charring Material Thermal Response and Ablation Program", Acurex Corporation, Aerotherm Division, Mountain View, CA, November 1987.

[16]Hutchinson, Virgil, et al. "Tempest: Crew Exploration Vehicle Concept," AIAA 2005-4190, 2005.